Macromolecules
ARTICLE

Macromolecules **2010**, *43*, 2981–2989 **2981**
DOI: 10.1021/ma902735t

SCFT Study of Tiling Patterns in ABC Star Terpolymers

Guojie Zhang, Feng Qiu,* Hongdong Zhang, and Yuliang Yang

The Key Laboratory of Molecular Engineering of Polymers, Ministry of Education, Department of Macromolecular Science, Fudan University, Shanghai 200433, China

An-Chang Shi*

Department of Physics and Astronomy, McMaster University, Hamilton, Ontario L8S 4M1, Canada

Received December 11, 2009; Revised Manuscript Received February 11, 2010

ABSTRACT: Ordered phases of ABC star terpolymer melts are investigated using a generic reciprocal-space implementation of the self-consistent field theory (SCFT) of polymers. The most important feature of ABC star triblock terpolymers is that their three blocks are joined at one junction point. This distinct topology of ABC star terpolymers constraints the junction points in one-dimensional lines in an ordered phase, resulting novel microphase-separated morphologies such as tiling patterns. Two types of star triblock terpolymers, with symmetric and asymmetric interaction parameters, are studied in detail. A variety of tiling patterns in ABC star terpolymers have been predicted from the SCFT calculation and relevant phase diagrams have been constructed. The predicted phase transition sequences from the SCFT calculations are in qualitative agreement with experimental and Monte Carlo simulation results.

I. Introduction

Ordered phases formed by block copolymers have attracted great attention in the last few decades. From a fundamental point of view, ordering in block copolymers melts or solutions provides an ideal paradigm for the study of self-organization in soft condensed matter.[1] From a technological point of view, the rich and fascinating ordered structures from block copolymers have found applications ranging from thermoplastic elastomers and high-impact plastics to pressure-sensitive adhesives, additives, foams. Furthermore, the ordered morphologies of block copolymers have potential applications in advanced technologies such as information storage, drug delivery, and photonic crystals.[2]

Previous studies have firmly established that the self-assembly of block copolymer melts is governed by a delicate balance of the interaction energy and chain conformational entropy.[3,4] For the simplest case of linear AB diblock copolymers, the equilibrium morphologies are governed by three parameters: the volume fraction of the A block, f_A, the AB interaction parameter χ, and the degree of polymerization, N. It is now well established that five stable ordered phases can be formed by AB diblock copolymers: alternating lamellae (L), hexagonally packed cylinders (C), spheres packed in a body-centered cubic or face-centered cubic lattice (S), double-gyroid network (G) and orthorhombic *Fddd* network (O^{70}).[5,6]

More complex block architectures, such as ABC triblock terpolymers, offer opportunities to create novel microphase morphologies. The richness of ordered structures in triblock terpolymers stems from a greatly enlarged parameter space. At the mean-field level, there are at least five independent molecular parameters determining the phase behavior of ABC triblock terpolymers: two independent compositions, i.e., volume fractions of A and B blocks, f_A and f_B, and three effective interaction parameters, $\chi_{AB}N$, $\chi_{BC}N$, and $\chi_{AC}N$. Furthermore, chain topology, namely, linear versus nonlinear triblock terpolymers (star-shaped, comb- and branched-type), or block sequence in linear triblock terpolymers, can also play important roles in determining the equilibrium structure. Consequently, much more complex morphologies can be obtained in ABC triblock terpolymers. To date more than three-dozen ordered structures have been identified in ABC linear triblock terpolymers.[7−9]

One distinct feature of ABC star triblock terpolymer is that, when the three blocks segregate, the topology of the chains forces the junction points of the three blocks to be in one-dimensional (1D) lines. In contrast, for ABC linear triblock terpolymers, the junctions of the AB and BC blocks are confined in two-dimensional (2D) surfaces in phase-separated structures. Because of the topological constraint, ABC star triblock terpolymers exhibit remarkably different phase behavior when compared with their linear counterpart. In general, either two-dimensional or three-dimensional (3D) ordered morphologies can be found in ABC star triblock terpolymer melts. Particularly, if the volume fractions of the three blocks are comparable, the junction points will most likely be arranged on straight lines, resulting in 2D ordered structures. In these 2D phases the three types of domains all assume the shape of cylinders with polygonal cross sections. These morphologies are therefore equivalent to 2D polygonal tiling patterns, or archimedean tiling.[10] The tiling patterns can be denoted by a set of integers [k, l, m, ...], indicating that a k-gon, an l-gon, and an m-gon, etc., meet consecutively at each vertex in the tiling pattern.

Experimental studies of star ABC terpolymers began to emerge in past decade.[11−15] In particular, Matsushita and coworkers have conducted systematic studies on the morphologies formed from (polyisoprene−polystyrene−poly(2-vinylpyridine)) (ISP) star terpolymers. Several ordered tiling patterns, such as [6.6.6], [8.8.4], [12.6.4], etc., have been observed in star ISP melts.[11−14] Furthermore, transformation from one structure to another was realized by varying the volume fraction of one component while keeping the composition ratio of the others fixed. Experiments by Abetz et al.[15] on polystyrene−polybutadiene−poly(2-vinylpyridine) (SBP) star terpolymers represent another

*Corresponding authors. E-mail: (F.Q.) fengqiu@fudan.edu.cn; (A.-C.S.) shi@mcmaster.ca.

© 2010 American Chemical Society

Published on Web 02/19/2010

typical system of star terpolymer, in which similar tiling structures were also observed.

Besides experimental works, computer simulations contribute a lot to understanding phase behaviors of ABC star terpolymers. Gemma and co-workers[16] carried out Monte Carlo (MC) simulations on ABC star terpolymers with equal interactions between the three components. The phase behavior of ABC star terpolymers with volume ratio of A:B:C = 1:1:x was investigated in detail in strong segregation region. Tiling patterns including [8.8.4], [6.6.6], [8.6.4; 8.6.6], [10.6.4; 10.6.4; 10.6.6], [12.6.4] were obtained from the MC simulations. Huang et al.[17] studied the effects of composition and interaction parameter on the phase behavior of ABC star terpolymers using dissipative particle dynamics simulations. Tiling patterns, such as [8.8.4], [6.6.6], [10.6.4;10.6.6], [10.6.4;10.8.4], were obtained when the three blocks have comparable volume fractions.

Despite the large amount of previous experiments and simulation studies on microphase separation of star terpolymer melts, a comprehensive understanding of the phase behavior of ABC star terpolymers is still lacking. Therefore, further systematic study on the phases and phase transitions of star terpolymers is desirable. It is now well established that self-consistent field theory (SCFT) has provided a powerful theoretical framework for the study of block polymer thermodynamics.[18,19] Historically, SCFT of polymers has its origin in the work of Edwards in the 1960s.[20] Delicate description of theoretical framework of SCFT for multicomponent polymers (including block copolymers and polymer blends) has been attributed to Helfand, Noolandi et al.[21,22] The first exact 3D numerical solution of the SCFT equations was attributed to the milestone work by Matsen and Schick, in which SCFT equations were solved using spectral method.[23] The availability of the exact numerical solutions allowed precise calculations of free energies and phase diagrams for block copolymers. In parallel, real-space method was established, including the Drolet−Fredrickson real-space method[24] and split-step method (or pseudospectral method) proposed by Rasmussen et al.[25] The capability and power of SCFT have been justified by fruitful applications in prediction of ordered phases and construction of phase diagrams of ABC linear triblock terpolymers.[26,27]

In this paper, we study phase behavior of ABC star terpolymers using a generic reciprocal-space implementation of SCFT equations.[27] To simplify the calculation and in response to results from previous experiments and simulations, the current SCFT calculation is carried out only in 2D space, where 2D tiling patterns are resulted. Various tiling patterns are predicted, and phase diagrams are constructed.

II. Theory

A. Partition Function and Free Energy. Our model system is composed of n ABC star terpolymers contained in a finite volume V. The size of the three blocks are characterized by their degree of polymerization, N_A, N_B, and N_C. Then, the overall molecular size of the star block terpolymer is characterized by $N = N_A + N_B + N_C$. The volume fractions of the A-, B- and C-monomers are $f_A = N_A/N$, $f_B = N_B/N$, and $f_C = 1 - f_A - f_B$, respectively. For simplicity, the A, B, and C monomers are assumed to have the same volume $v_0 = 1/\rho_0$, where the monomer density, ρ_0, is defined as the number of monomers per unit volume. The statistical segment lengths of each component are denoted as b_α (α = A, B, or C). The conformation of the three blocks (subchains or arms) is described by a space curve, $\mathbf{R}_i^\alpha(s)$, which specifies the spatial position of the s-th monomer of the α-block in the ith chain. The three arms are connected by one monomer indexed by $s = 0$. Therefore, the conformation of the A, B, and C arms are specified by $\mathbf{R}^A(s)$ with $s \in [0, f_A]$, $\mathbf{R}^B(s)$ with $s \in [0, f_B]$, and $\mathbf{R}^C(s)$ with $s \in [0, f_C]$, respectively.

The partition function of the system under consideration is given as a summation over all the chain conformations,

$$Z_C \sim \int \mathscr{D}\{\mathbf{R}(\bullet)\} P_0(\{\mathbf{R}(\bullet)\}) \prod_{\mathbf{r}} \delta[1 - \sum_\alpha \hat{\phi}_\alpha(\mathbf{r})] \exp[-V(\{\hat{\phi}\})/k_B T] \quad (1)$$

where $\{\mathbf{R}(\bullet)\}$ specifies the chain conformation, defined by $\{\mathbf{R}_1(\bullet), \mathbf{R}_2(\bullet), ..., \mathbf{R}_n(\bullet)\}$ ($\mathbf{R}_i(\bullet)$ represents the conformation of i-th chain), and $P_0(\{\mathbf{R}(\bullet)\})$ is the probability distribution of a given chain conformation,

$$P_0(\{\mathbf{R}(\bullet)\}) = \prod_{i=1}^{n} \{p_0(\mathbf{R}_i(\bullet)) \delta[\mathbf{R}_i^A(0) - \mathbf{R}_i^B(0)] \delta[\mathbf{R}_i^A(0) - \mathbf{R}_i^C(0)]\} \quad (2)$$

where

$$p_0(\mathbf{R}(\bullet)) = A \exp\left[-\sum_\alpha \frac{3}{2Nb_\alpha^2} \int_0^{f_\alpha} \mathrm{d}s \left(\frac{\mathrm{d}\mathbf{R}^\alpha(s)}{\mathrm{d}s} \right)^2 \right] \quad (3)$$

$V(\{\hat{\phi}\})$ in eq 1 is the monomer interaction functional, which is often written in terms of the Flory−Huggins interaction parameters,

$$V(\{\hat{\phi}\}) = \frac{1}{2} k_B T \sum_\alpha \sum_{\beta \neq \alpha} \chi_{\alpha\beta} \rho_0 \int \mathrm{d}\mathbf{r}\, \hat{\phi}_\alpha(\mathbf{r}) \hat{\phi}_\beta(\mathbf{r}) \quad (4)$$

The dimensionless density distribution function of A-monomer is defined as

$$\hat{\phi}_A(\mathbf{r}) = \frac{N}{\rho_0} \sum_{i=1}^{n} \int_0^{f_A} \mathrm{d}s\, \delta(\mathbf{r} - \mathbf{R}_i^A(s)) \quad (5)$$

and $\hat{\phi}_B$ and $\hat{\phi}_C$ have a similar expression.

The self-consistent field theory of block copolymers starts with inserting a functional integral

$$1 = \int \mathscr{D}\{\phi_\alpha\} \delta(\phi_\alpha - \hat{\phi}_\alpha)$$

into eq 1. This mathematical manipulation permits the replacement of the density operator $\hat{\phi}_\alpha(\mathbf{r})$ in eq 1 by the density field $\phi_\alpha(\mathbf{r})$. Then, the partition function can be written as,

$$Z_C \sim \int \prod_\alpha [\mathscr{D}\{\phi_\alpha\} \mathscr{D}\{\omega_\alpha\}] \prod_{\mathbf{r}} \delta[1 - \sum_\alpha \phi_\alpha(\mathbf{r})] \exp[-F_C(\{\phi\}, \{\omega\})/k_B T] \quad (6)$$

where the functional F_C is given by

$$F_C(\{\phi\}, \{\omega\}) = \frac{\rho_0 R_g^3 k_B T}{N} \left\{ -V \ln Q_C + \int \mathrm{d}\mathbf{r} \left[\frac{1}{2} \sum_\alpha \sum_{\beta \neq \alpha} \chi_{\alpha\beta} N \phi_\alpha(\mathbf{r}) \phi_\beta(\mathbf{r}) - \sum_\alpha \omega_\alpha(\mathbf{r}) \phi_\alpha(\mathbf{r}) \right] \right\} \quad (7)$$

Here, the single-chain partition function is defined as:

$$Q_C(\{\omega\}) \equiv \frac{1}{V} \int \mathscr{D}\{\mathbf{R}(\bullet)\} P_0\{\mathbf{R}(\bullet)\} \exp[-\sum_\alpha \int_0^{f_\alpha} \mathrm{d}s\, \omega_\alpha(\mathbf{R}^\alpha(s))] \quad (8)$$

We define the "forward" and "backward" end-integrated chain propagators:

$$q_\alpha(\mathbf{r},s) \equiv \int d\mathbf{r}' \int \mathscr{D}\{\mathbf{R}(\bullet)\}P_0\{\mathbf{R}(\bullet)\} \exp[-\int_0^{f_\alpha} ds\, \omega_\alpha(\mathbf{R}^\alpha(s))]\delta[\mathbf{r}-\mathbf{R}^\alpha(s)]\delta[\mathbf{r}'-\mathbf{R}^\alpha(0)] \quad (9)$$

$$q_\alpha^\dagger(\mathbf{r},s) \equiv \int d\mathbf{r}' \int \mathscr{D}\{\mathbf{R}(\bullet)\}P_0\{\mathbf{R}(\bullet)\} \exp[-\int_0^{f_\alpha} ds\, \omega_\alpha(\mathbf{R}^\alpha(s))]\delta[\mathbf{r}-\mathbf{R}^\alpha(s)]\delta[\mathbf{r}'-\mathbf{R}^\alpha(f_\alpha)] \quad (10)$$

Then they satisfy the differential modified diffusion equations

$$\frac{\partial}{\partial s}q_\alpha(\mathbf{r},s) = \left[\frac{1}{6}Nb^2\nabla^2 - \omega_\alpha(\mathbf{r})\right]q_\alpha(\mathbf{r},s) \quad (11)$$

$$\frac{\partial}{\partial s}q_\alpha^\dagger(\mathbf{r},s) = -\left[\frac{1}{6}Nb^2\nabla^2 - \omega_\alpha(\mathbf{r})\right]q_\alpha^\dagger(\mathbf{r},s) \quad (12)$$

Under the saddle-point approximation, minimization of free energy functional leads to the following set of SCFT equations:

$$\phi_A(\mathbf{r}) = \frac{1}{Q_C}\int_0^{f_A} ds\, q_A(\mathbf{r},s)q_A^\dagger(\mathbf{r},s)$$

$$\phi_B(\mathbf{r}) = \frac{1}{Q_C}\int_0^{f_B} ds\, q_B(\mathbf{r},s)q_B^\dagger(\mathbf{r},s)$$

$$\phi_C(\mathbf{r}) = \frac{1}{Q_C}\int_0^{f_C} ds\, q_C(\mathbf{r},s)q_C^\dagger(\mathbf{r},s)$$

$$\omega_A(\mathbf{r}) = \chi_{AB}N\phi_B(\mathbf{r}) + \chi_{AC}N\phi_C(\mathbf{r}) + \eta(\mathbf{r})$$

$$\omega_B(\mathbf{r}) = \chi_{AB}N\phi_A(\mathbf{r}) + \chi_{BC}N\phi_C(\mathbf{r}) + \eta(\mathbf{r})$$

$$\omega_C(\mathbf{r}) = \chi_{AC}N\phi_A(\mathbf{r}) + \chi_{BC}N\phi_B(\mathbf{r}) + \eta(\mathbf{r}) \quad (13)$$

where $\eta(\mathbf{r})$ is introduced to ensure the incompressibility condition: $\sum_\alpha \phi_\alpha(\mathbf{r}) = 1$. Solutions of this set of SCFT equations correspond to different phases of the system. Phase diagrams can be constructed by comparing the free energy of the different solutions.

Three different numerical methods, including the spectral method,[23] the real-space method,[24] and the pseudospectral method,[25] have been established to solve the SCFT equations during the past few decades. The spectral method found its applications in determination with high precision of free energies of known ordered phases and thus construction of phase diagrams. The real-space method and pseudospectral method are powerful in searching unknown phases of block copolymers. As an alternative, in the following, we solve the SCFT equations of ABC star terpolymers using a generic reciprocal-space method, which is a straightforward extension of our previous work.[27]

B. Reciprocal Formulation. The SCFT framework presented above is developed in real space. Mathematically, any spatially varying functions can be represented in the Fourier space. Therefore, the SCFT can be cast in the reciprocal space. Specifically, the functions of interest within the SCFT, such as the mean-field concentrations, the mean-field potentials, and the end-integrated propagators, are expanded in terms of Fourier series. The SCFT is then cast in terms of the expansion coefficients.

Solving SCFT equations in reciprocal-space starts with expanding the functions of interest using the plane waves, $e^{i\mathbf{G}\mathbf{r}}$, as the basis functions. The wave vector $\mathbf{G}$ is determined by specific discretization of the reciprocal space. One useful method to discretize the reciprocal space is to use periodic boundary conditions applied to the computation box with specific size and shape. Once the reciprocal vectors are specified, any spatially varying functions of interest, $\psi_\alpha(\mathbf{r})$, can be expressed in terms of Fourier series as

$$\psi_\alpha(\mathbf{r}) = \sum_j \psi_{\alpha,j}e^{i\mathbf{G}_j\cdot\mathbf{r}} \quad (14)$$

Here, we only discuss cases in a rectangular computation box.[28] In this case the wave vector $\mathbf{G}$ is defined by $\mathbf{G} = 2\pi(h/D_x, k/D_y, l/D_Z$, where D_x, D_y, D_z are the sizes of the rectangular box, and h, k, l are integers. Thus, a reciprocal wave vector can be represented by a set of integers (h, k, l). In SCFT calculations, the wave vectors $\mathbf{G}$ are ordered such that $|\mathbf{G}|$ forms a nondecreasing series, therefore the first wave vector is $\mathbf{G}_1 = \vec{0}$.

Then, the modified diffusion equations, eqs 11 and 12, are rewritten in reciprocal-space as

$$\frac{\partial q_{\alpha,i}(s)}{\partial s} = -\sum_j H_\alpha(\mathbf{G}_i,\mathbf{G}_j)q_{\alpha,j}(s) \quad (15)$$

$$\frac{\partial q_{\alpha,i}^\dagger(s)}{\partial s} = \sum_j H_\alpha(\mathbf{G}_i,\mathbf{G}_j)q_{\alpha,j}^\dagger(s) \quad (16)$$

with the initial conditions

$$q_{\alpha,i}^\dagger(f_\alpha) = \delta_{\mathbf{G}_i,\mathbf{G}_1}, q_{\beta,i}^\dagger(f_\beta) = \delta_{\mathbf{G}_i,\mathbf{G}_1}, q_{\gamma,i}(0) = \sum_j q_{\alpha,j}^\dagger(0)\sum_k q_{\beta,k}^\dagger(0)\delta_{\mathbf{G}_i,\mathbf{G}_j+\mathbf{G}_k} \quad (17)$$

where the Hamiltonians are

$$H_\alpha(\mathbf{G}_i,\mathbf{G}_j) = \frac{1}{6}Nb^2\mathbf{G}_i{}^2\delta_{\mathbf{G}_i,\mathbf{G}_j} + \sum_k \omega_{\alpha,k}(s)\delta_{\mathbf{G}_i,\mathbf{G}_j+\mathbf{G}_k} \quad (18)$$

The solution to the above first-order linear ordinary differential equation is given by

$$q_{\alpha,i}(s) = \sum_j T_{\alpha,ij}(s)q_{\alpha,j}(0) \quad (19)$$

where $\mathbf{T}_\alpha(s) = \exp[-\mathbf{H}_\alpha s]$ is a transfer matrix. Because the Hamiltonian $\mathbf{H}$ is an Hermitian matrix, diagonalization of matrix $\mathbf{H}$ can be performed, $\mathbf{H}_\alpha = \mathbf{U}_\alpha\mathbf{D}_\alpha\mathbf{U}_\alpha^\dagger$, where the elements of the diagonal matrix $\mathbf{D}_\alpha$, $d_{\alpha,k} \equiv D_{\alpha,kk}$, are real eigenvalues of $\mathbf{H}_\alpha$, and the columns of $\mathbf{U}_\alpha$ are the normalized eigenvectors of $\mathbf{H}_\alpha$.

The transfer matrix can be expressed as $\mathbf{T}_\alpha(s) = \mathbf{U}_\alpha \exp[-\mathbf{D}_\alpha s]\mathbf{U}_\alpha^\dagger$, with its elements

$$T_{\alpha,ij}(s) = \sum_k U_{\alpha,ik} \exp[-d_{\alpha,k}s] U^\dagger_{\alpha,kj} \tag{20}$$

Starting from the initial conditions of the coefficients of the "backward" end-integrated chain propagators

$$q^\dagger_{\alpha,i}(f_\alpha) = \delta_{\mathbf{G}_i,\mathbf{G}_1} \tag{21}$$

the coefficients for the "backward" end-integrated chain propagators expanded in terms of the eigenvalues and eigenfunctions are obtained as,

$$q^\dagger_{\alpha,i}(s) = \sum_j U_{\alpha,ij} \exp(-d_{\alpha,j}(f_\alpha - s)) U^\dagger_{\alpha,i1} \quad \text{for star } \alpha,\ 0 \le s \le f_\alpha \tag{22}$$

Because of the topological constraint that three chemically distinct chains are connected into a common junction ($s = 0$) in ABC star terpolymers, specific initial conditions $q_{A,i}(0)$, $q_{B,i}(0)$, $q_{C,i}(0)$ for solving the 'forward' end-integrated chain propagators equations must be satisfied

$$\begin{aligned} q_{A,i}(0) &= \sum_j q^\dagger_{B,j}(0) \sum_k q^\dagger_{C,k}(0) \delta_{\mathbf{G}_i,\mathbf{G}_j+\mathbf{G}_k} \\ q_{B,i}(0) &= \sum_j q^\dagger_{C,j}(0) \sum_k q^\dagger_{A,k}(0) \delta_{\mathbf{G}_i,\mathbf{G}_j+\mathbf{G}_k} \\ q_{C,i}(0) &= \sum_j q^\dagger_{A,j}(0) \sum_k q^\dagger_{B,k}(0) \delta_{\mathbf{G}_i,\mathbf{G}_j+\mathbf{G}_k} \end{aligned} \tag{23}$$

Then, we get the "forward" chain propagators,

$$q_{\alpha,i}(s) = \sum_j \sum_k U_{\alpha,ik} \exp(-d_{\alpha,k}s) U^\dagger_{\alpha,kj} q_{\alpha,j}(0) \quad \text{for arm } \alpha,\ 0 \le s \le f_\alpha \tag{24}$$

The density profiles are written as

$$\phi_{\alpha,i} = \frac{1}{Q_C} \sum_j \sum_k \int_0^{f_\alpha} \mathrm{d}s\, q_{\alpha,j}(s) q^\dagger_{\alpha,k}(s) \delta_{\mathbf{G}_i,\mathbf{G}_j+\mathbf{G}_k} \tag{25}$$

The component density coefficients are also expressed in terms of the eigenvalues and eigenvectors

$$\phi_{\alpha,i} = \frac{1}{Q_C} \sum_j \sum_k \delta_{\mathbf{G}_i,\mathbf{G}_j+\mathbf{G}_k} \sum_l \sum_m U_{\alpha,jm} U^\dagger_{\alpha,ml} q_{\alpha,l}(0) \sum_n U_{\alpha,kn} U^\dagger_{\alpha,n1} \frac{e^{-d_{\alpha,m}f_\alpha} - e^{-d_{\alpha,n}f_\alpha}}{d_{\alpha,n} - d_{\alpha,m}} \tag{26}$$

The free energy can be written as

$$\frac{F_C}{nk_BT} = -\ln Q_C + \sum_i \sum_j [\chi_{AB}N\phi_{A,i}\phi_{B,j} + \chi_{BC}N\phi_{B,i}\phi_{C,j} + \chi_{AC}N\phi_{A,i}\phi_{C,j}]\delta_{\mathbf{G}_i,-\mathbf{G}_j} \tag{27}$$

with the single-chain partition function

$$Q_C = \sum_i \sum_j q_{\alpha,i}(0) q^\dagger_{\alpha,j}(0) \delta_{\mathbf{G}_i,-\mathbf{G}_j} \tag{28}$$

The fields $\omega_{\alpha,i}$ are determined self-consistently from

$$\begin{aligned} \omega_{A,i} &= \chi_{AB}N\phi_{B,i} + \chi_{AC}N\phi_{C,i} + \eta_i \\ \omega_{B,i} &= \chi_{AB}N\phi_{A,i} + \chi_{BC}N\phi_{C,i} + \eta_i \\ \omega_{C,i} &= \chi_{AC}N\phi_{A,i} + \chi_{BC}N\phi_{B,i} + \eta_i \\ \phi_{A,i} + \phi_{B,i} + \phi_{B,i} &= \delta_{\mathbf{G}_i,\mathbf{G}_1} \end{aligned} \tag{29}$$

where the field η ensures the incompressibility of the system and is determined by

$$\eta_i = \frac{C_1C_2(\omega_{A,i} + \omega_{C,i}) + C_2C_3(\omega_{A,i} + \omega_{B,i}) + C_1C_3(\omega_{B,i} + \omega_{C,i})}{2(C_1C_2 + C_2C_3 + C_1C_3)} \tag{30}$$

with

$$\begin{aligned} C_1 &= \chi_{AC} + \chi_{BC} - \chi_{AB} \\ C_2 &= \chi_{AC} + \chi_{AB} - \chi_{BC} \\ C_3 &= \chi_{AB} + \chi_{BC} - \chi_{AC} \end{aligned} \tag{31}$$

C. Scattering Intensity. In this section, a brief description of the method to compute the scattering intensity of an ordered phase from the SCFT solutions is given. In general, the scattering intensity of block copolymer microphases is composed of two contributions. The first and main contribution is from a set of Bragg peaks whose amplitudes can be determined from the mean-field solution of SCFT. The second contribution is from composition fluctuations that are absent in the current SCFT studies. In what follows, we investigate the scattering intensity from the first contribution. For ordered phases formed by ABC star triblocks, the scattering intensity $I(\mathbf{q})$ is given by

$$I(\mathbf{q}) = \sum_{\alpha=A,B,C} \sum_{\beta=A,B,C} U_\alpha(\mathbf{q}) U^*_\beta(\mathbf{q}) \phi_\alpha(\mathbf{q}) \phi^*_\beta(\mathbf{q}) \tag{32}$$

where $U_\alpha(\mathbf{q})$ is the atomic form factor of the component α.[29] For simplicity, we assume that the atomic form factors for each component are equal to a same constant. In eq 32, $\phi_\alpha(\mathbf{q})$ is the coefficient of α species for the wave vector $\mathbf{q}$ in reciprocal-space, while $\phi^*_\beta(\mathbf{q})$ is the complex conjugate of the coefficients of β species for the wave vector $\mathbf{q}$ in reciprocal-space.

III. Results and Discussion

In the ordered phases of star triblock polymers, the most distinct feature is that the junction points of the terpolymers are forced to be along one-dimensional lines, as a result of the topological constraint that the three blocks must meet at one junction point. In general, the lines of junctions can be either straight or curved, depending on the relative lengths of the three arms and the interactions among them. The structure of the ordered phases is basically determined by the arrangement of these lines of junctions. When the lines of junctions are straight,

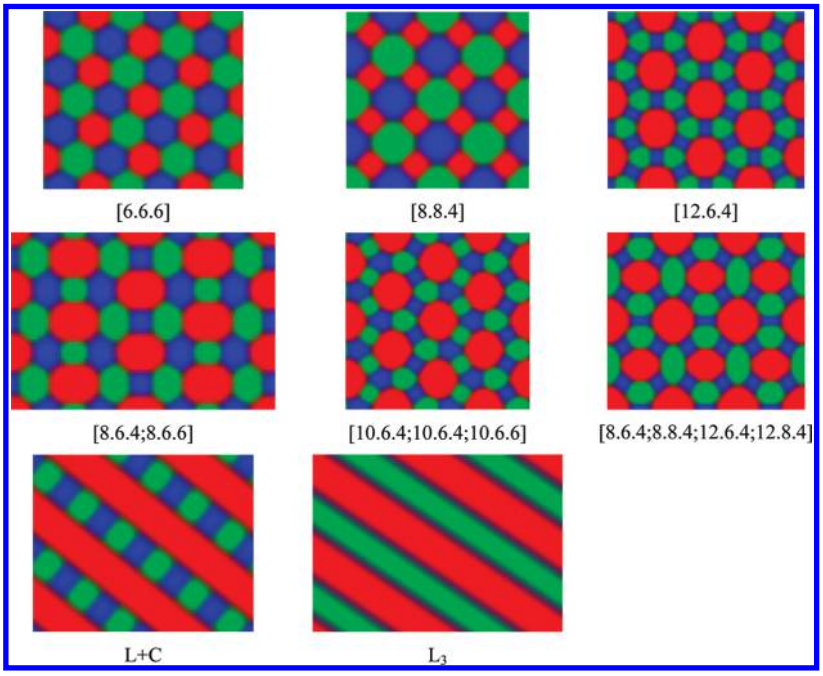

Figure 1. Ordered phases of ABC star triblock terpolymers obtained using SCFT with Fourier-space method. The structures shown are schematics that have been reconstructed from the nonzero Fourier weights of the density distribution functions of monomers A, B, and C, denoted by blue, green, and red colors.

typically found in relatively strong segregated system with approximately equal volume factions of the blocks, 2D phases or tiling patterns are formed. When the lines of junctions are curved, complex 3D phases are obtained. In previous experimental and simulation studies, much attention has been focused on 2D tiling patterns. Motivated by these previous studies, the main focus of this paper is on tiling patterns formed by ABC star terpolymers, therefore all calculations are carried out in 2D space. Each calculation starts with a random guess of the solution, then a relaxation method is applied until the maximum changes of the field coefficient at each iteration are reduced to 10^{-4} (corresponding to a free energy change of 10^{-6}).[30] All SCFT calculations are carried out in single unit cell. For a given phase, its free energy is minimized with respect to the box parameters (D_x, D_y, all in units of R_g). Specifically, the box parameters, D_x and D_y, are tuned independently in the range 3.0−10.8.

In all reciprocal-space calculations 151 basis functions are used. In principle, the accuracy of the reciprocal-space method is determined by the number of basis function used. To clarify whether 151 basis functions in the reciprocal-space method are sufficient to achieve quantitative accuracy, we have calculated the free energies of a few typical phases in ABC star terpolymers using both generic reciprocal-space method and Matsen−Schick method. The relative differences in free energy are below 1% in weak to intermediate segregation region, although the errors increase with higher interaction parameter. For cases of χN = 30.0 in present work, the differences are within 0.2%, which provides adequate accuracy for screening phases.

The spatial resolution is also determined by the number of basis functions used. According to eq 14, in 2D space, integer h (k) in wave vector $\mathbf{G} = 2\pi(h/D_x, k/D_y)$ can be viewed as the number of period of basis functions in length D_x (D_y). Consequently, a basis function with $\mathbf{G} = 2\pi(h/D_x, k/D_y)$ has the ability to resolute structural change on the length scale of $D_x/2h$ ($D_y/2k$) in the x-direction (y-direction). Therefore, the highest values of h, k determine the degree of spatial resolution. In our 2D calculations, 151 basis functions are used, which means the largest value of h and k in all basis functions can be 9 and 5, respectively. As a result, spatial resolution is estimated to be on the scale of $D_x/18$, $D_y/10$; we believe this is enough to represent a unit cell of tiling patterns for the purpose of screening phases in intermediate segregation region.

(I). Two-Dimensional Tiling Patterns. Before presenting the detailed results, it is useful to introduce the notations. In what follows, $A_xB_yC_z$ represents the ABC star terpolymers with a composition ratio of A:B:C = x:y:z. When the lengths of the star-arms are long and approximately equal to each other, the star terpolymers tend to self-assemble into parallel cylinders with polygonal cross sections, which can be characterized as 2D tiling patterns. As mentioned in the Introduction, the tiling patterns can be represented by a set of integers, [k, l, m, ...]. The integers indicate that the k-gon, l-gon, m-gon, etc., meet consecutively at each vertex. Examples of different tiling patterns found in ABC star terpolymers and their integer designations are shown in Figure 1. The first pattern is designated as [6.6.6] because each vertex in this pattern is surrounded by three hexagonal polygons. Similarly the second and third patterns are designated as [8.8.4] and [12.6.4], respectively. The fourth pattern represents a more complex case because it possesses two types of vertices; one is surrounded by 8-gon, 6-gon, and 4-gon, whereas the other is formed by an 8-gon and two 6-gons. Consequently, this pattern is designated as [8.6.4;8.6.6]. Similarly, the fifth pattern has three types of vertices and it is in turn designated as [10.6.4;10.6.4;10.6.6], and the sixth pattern in Figure 1 is termed [8.6.4;8.8.4;12.6.4;12.8.4].

In the present study, a number of ordered 2D morphologies (tiling patterns) have been obtained from the SCFT calculations. In what follows, a brief description of these phases is given first. Detailed discussions on the phase behavior of ABC star triblock terpolymers are presented later.

(1) [6.6.6]: This pattern has the same structure as the honeycomb structure and it is a typical ordered phase of ABC star terpolymers. In this pattern, the three components exhibit hexagonal microdomains and the pattern has a 3-fold symmetry. This structure is an example of noncentrosymmetric phases.

(2) [8.8.4]: The unit cell of this pattern contains two octagonal domains formed by two different arms and one 4-coordinated domain formed by the third arm. It should be noted that the two octagonal microdomains do not need to have the same size, and the 4-coordinated microdomains can deviate from squares. Details of these microdomains are determined by the volume fractions of the three blocks.

(3) [8.6.4;8.6.6]: In this pattern, two types of 8-coordinated domains formed by the longest arm (the C-block) are surrounded by domains formed alternatively by the other two arms (the A and B blocks). The A and B blocks form two types of microdomains with different shapes and sizes, i.e., the 4- and 6-coordinated polygons. The unit cell of this phase is nonprimitive, composed of one 4-coordinated A-domain, two 6-coordinated B-domains and two types of 8-coordinated C-domains.

(4) [10.6.4;10.6.4;10.6.6]: In this pattern, the longest arms (C-blocks) form ten-coordinated domains, which are surrounded alternatively by A and B microdomains. An interesting feature of the A and B domains is that they represent two types of microstructures with different shapes and sizes. We note that this pattern is also a noncentrosymmetric phase.

(5) [8.6.4;8.8.4;12.6.4;12.8.4]: For this pattern, the longest blocks form two types of domains: 12-coordinated polygons and 8-corrdinated polygons. On the other hand, microdomains formed by the shortest blocks have rectangular sections but with different sizes. Similarly, the blocks with intermediate-length form two types of polygons with different sizes, 6- and 8-coordinated polygons.

(6) [12.6.4]: In this phase, the longest blocks are surrounded by 12 microdomains of the other two blocks arranged alternatively. One of the shorter blocks form nearly hexagonal polygons, while the other blocks form rectangular structure.

(7) L + C: In this pattern, the longest block (i.e., C block) forms lamellar layers, whereas the two shorter blocks (i.e., A and B blocks) form cylinders with rectangular cross-section and arranged alternatively between C lamellae.

(8) L_3: In this pattern, lamellae formed by the shortest blocks are sandwiched in between two lamellae formed by the other two components.

A. Symmetric Interaction Parameters. In order to highlight the influence of composition on the self-assembled equilibrium morphologies, we first investigate the phase behavior of a model ABC star terpolymer with symmetric interaction parameters ($\chi_{AB}N = \chi_{BC}N = \chi_{AC}N = 30.0$) and equal statistical segment lengths ($b_A = b_B = b_C$). Because the incompatibility between the different blocks is relatively large, we expect that cylindrical phases or tiling patterns will form in this model terpolymer.

A one-dimensional phase map of the star terpolymer $A_{1.0}B_{1.0}C_x$ as a function of x is shown in Figure 2, in which three colors, blue, green and red, are used to represent the A, B, and C blocks, respectively. The increment of the volume fraction f_A (or f_B) in the phase diagram is 0.001. Equilibrium phases are assigned by comparing the free energies of the candidate structures listed above. With the increase of f_C from 0.210 to 0.500 ($0.53 < x < 2.02$), phase transformation occurs in the sequence of [8.8.4], [6.6.6], [8.6.4;8.6.6], [10.6.4;10.6.4;10.6.6]. A detailed description, explanation,

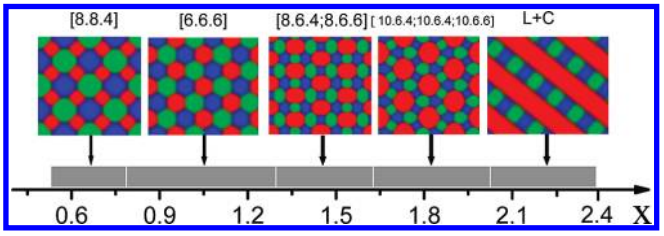

Figure 2. Phase behavior of an idealized $A_{1.0}B_{1.0}C_x$ star triblock terpolymer with symmetric interactions, $\chi_{AB}N = \chi_{BC}N = \chi_{AC}N = 30.0$, and with equal statistical segment lengths for each block. The structures shown are schematics that have been reconstructed from the nonzero Fourier weights of the density distribution functions of monomers A, B, and C, denoted by blue, green, and red colors.

and comparison with relevant results from MC simulations are presented below.

When the volume fraction of the C-block is in the range $0.210 \le f_C \le 0.280$ (or $0.53 < x < 0.79$), the pattern [8.8.4] is found to be stable. In this structure, the microdomains formed by either A or B blocks are octagonal with equal size, while the C-domains display square-like sections. These results are in good agreement with the observation from MC simulation by Gemma et al.,[16] in which the [8.8.4] cylinders were found to appear in the region $0.37 \le x \le 0.70$. However, this tiling pattern has not been observed experimentally at present time.

When x is increased to values larger than 0.79, the SCFT predicts that the honeycomb-like morphology ([6.6.6] tiling pattern) becomes stable. The honeycomb tiling is a characteristic noncentrosymmetric structure for ABC star triblock terpolymers. This structure is found to be stable in a wide region of $0.79 \le x \le 1.28$ ($0.280 \le f_C \le 0.390$), in agreement with the MC simulation result 16, in which [6.6.6] cylinders were found in the range $0.80 \le x \le 1.20$.

The tiling pattern [8.6.4;8.6.6] becomes stable when $1.28 \le x \le 1.62$ ($0.390 \le f_C \le 0.450$). Similar structure has been predicted in region of $1.50 \le x \le 1.75$ in previous MC simulations.[16]

For larger values of x ($1.62 \le x \le 2.02$, $0.450 \le f_C \le 0.500$), the [10.6.4;10.6.4;10.6.6] tiling pattern becomes the stable phase. The same pattern was found to be stable by MC simulations in this region ($x \approx 2.00$).[16]

The L + C structure becomes stable in the region of $x > 2.02$. However previous MC simulations predicted that the L + C pattern is located at larger values of x: $3 \le x \le 5$.

Since in most cases of Gemma et al.'s simulation, $\chi N = 54$ was used while we chose a lower χN value ($\chi N = 30$) to reduce the number of basis function needed, the reasonably good agreement between SCFT calculation and MC simulation reflects that phase behaviors of ABC star terpolymers with symmetric interactions are not sensitive to the change of interaction parameters in the intermediate segregation region. The discrepancy of the stability region for L + C phase may result from different interaction parameters used in SCFT and MC. Furthermore, Gemma et al.'s MC simulations were carried out in 3D space, in addition to 2D tiling patterns, interesting 3D morphologies were found at higher interaction parameters, including lamella + sphere ($\chi N > 100$), perforated layers, columnar piled disk ($\chi N = 77$) and lamellae in sphere ($\chi N \approx 100$). Such 3D structures will compete for stability with the L + C phase, which may also cause large discrepancy with the prediction of 2D SCFT.

The phase behavior of ABC star triblock terpolymers with equal interaction parameters $\chi_{AB}N = \chi_{BC}N = \chi_{AC}N = 30.0$ is summarized in a phase diagram shown in Figure 3. The phase diagram is constructed by comparing the free energy of

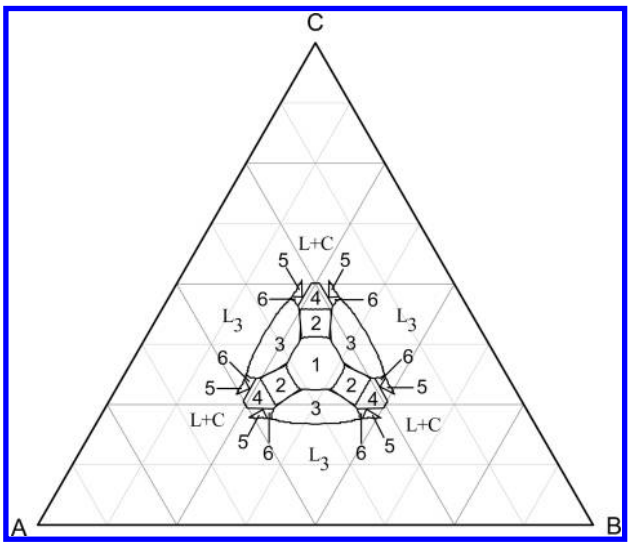

Figure 3. Partial phase triangle for a model ABC star triblock terpolymers with equal statistical segment lengths for each block and with equal interaction parameters, $\chi_{AB}N = \chi_{BC}N = \chi_{AC}N = 30.0$. The ordered phases obtained are indexed as numbers: 1, [6.6.6]; 2, [8.6.4;8.6.6]; 3, [8.8.4]; 4, [10.6.4;10.6.4;10.6.6]; 5, [12.6.4]; 6, [8.6.4;8.8.4; 12.6.4;12.8.4].

the different candidate structures using SCFT calculation with an increment of the volume fractions (f_A, f_B, f_C) of 0.001. In order to focus on the tiling patterns of ABC star polymers, the SCFT calculation is carried out for star terpolymers with compositions located near the center of the phase diagram, where the three star blocks have comparable lengths. Near the three edges of the triangle phase diagram, where one of the three arms is much shorter than the others, the ABC star terpolymers would exhibit phases typically formed from diblock copolymers. The phase diagram shown in Figure 3 is 3-fold symmetric due to symmetric interaction parameters used. A hexagonal region in the center of triangle phase diagram, in which the volume fractions of three species are nearly equal, is occupied by the tiling pattern [6.6.6]. Two types of tiling patterns, [8.6.4;8.6.6] and [8.8.4], are found near the [6.6.6] region. More complex tiling patterns, such as [10.6.4;10.6.4;10.6.6], [12.6.4], and [8.6.4;8.8.4;12.6.4;12.8.4], appear in regions where the volume fraction of one block is relatively larger than the other two blocks.

B. Asymmetric Interaction Parameters. In this section, we proceed to discuss the phase behavior of ABC star triblock terpolymers with asymmetric interaction parameters, largely motivated by experimental results on ISP star triblock terpolymers from Matsushita and co-workers.[11−14] In a series of investigations, three groups of ISP star terpolymers with fixed length ratio of two arms, $I_{1.0}S_{1.0}P_x$,[11−13] $I_{1.0}S_{1.8}P_x$,[14] and $I_{1.0}S_xP_{2.0}$,[14] were studied and many interesting microphase-separated structures have been observed, including the cylindrical phases (tiling patterns) of [6.6.6], [8.8.4], [10.6.4;10.6.4;10.6.6], [12.6.4], [3.3.4.3.4], and [8.6.4;8.6.6]. Many of these tiling patterns have been discussed in previous section. In order to make a meaningful comparison of the SCFT and experimental results, the interaction parameters are chosen so that they are appropriate for the ISP terpolymers. Although accurate values of the Flory−Huggins parameters for the ISP system are not available in the literature, qualitatively the interaction strengths are known to follow the order $\chi_{IS} \approx \chi_{SP} < \chi_{IP}$. In what follows we choose $\chi_{IS}N = \chi_{SP}N = 25.0$, $\chi_{IP}N = 37.0$ to model the ISP system. Following the experiments by Matsushita et al., we examine the phase behavior of the

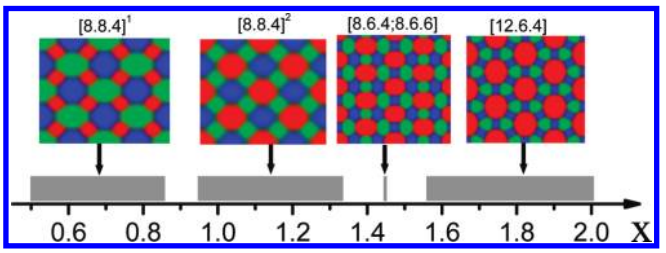

Figure 4. Equilibrium ordered morphologies of $A_{1.0}B_{1.0}C_x$ star triblock terpolymer with asymmetric interactions, $\chi_{AB}N = \chi_{BC}N = 25.0$, and $\chi_{AC}N = 37.0$, and with equal statistical segment lengths for each block. The structures shown are schematics that have been reconstructed from the nonzero Fourier weights of the density distribution functions of monomers A, B, and C, denoted by blue, green, and red colors.

$I_{1.0}S_{1.0}P_x$ series of star triblock terpolymers. The resulting SCFT phase diagram is shown in Figure 4 with an increment of volume fraction f_A of 0.01.

With the increase of f_C, the ordered stable microphase changes from $[8.8.4]^1$ to $[8.8.4]^2$ then to [8.6.4;8.6.6] and finally to [12.6.4]. We note that two types of [8.8.4] tiling patterns, $[8.8.4]^1$ and $[8.8.4]^2$, are obtained for the $A_{1.0}B_{1.0}C_x$ star terpolymers with $\chi_{AB}N = \chi_{BC}N = 25.0$, and $\chi_{AC}N = 37.0$. Obviously, the coordination number of C-domains is proportional to the value of x, increasing from 4, to 8, and then to 12 when x changes from 0.5 to 2.0. Compared to the case with symmetric interaction parameters, the asymmetric interactions between the three species lead to remarkable changes in the phase behavior. For example, the [6.6.6] tiling pattern now becomes metastable, and a previously metastable candidate [12.6.4] emerges as a stable one. Furthermore, in the phase diagram the stable area of each phase is also significantly changed. For asymmetric star polymers, the stable region of the [8.8.4] phase is greatly enlarged.

For star triblock terpolymers with shorter C-arms ($0.50 \leq x \leq 0.86$), a typical phase denoted as $[8.8.4]^1$ is formed (Figure 4). Although in the phase diagram a broad region is covered by the $[8.8.4]^1$ phase, this tiling pattern has not been observed in experiments. Instead, the [6.6.6] pattern was observed for $I_{1.0}S_{1.0}P_{0.7}$. In our studies, for $x \approx 0.86$, the pattern [6.6.6] is found to be a metastable phase with a higher free energy density.

In a large region of $0.94 \leq x \leq 1.33$, the $[8.8.4]^2$ tiling pattern becomes a stable phase. In the $[8.8.4]^2$ phase, the majority C-blocks form the 8-coordinated domains, which are surrounded by four B-block 4-polygons and four domains of A-blocks with 8-coordinations. Because of the larger interaction parameter between components A and C, B/C interface dominates the morphology. In contrast, the [6.6.6] pattern stays as a stable phase in this region for star terpolymers with symmetric interactions. The asymmetric interactions, however, drives the [6.6.6] pattern into a metastable one in this region. In the experiments,[11,12] the ISP star terpolymer with arm-length ratio 1:1:1.2 exhibits a similar $[8.8.4]^2$ phase. For $I_{1.0}S_{1.0}P_{1.2}$, the blocks with equal-lengths, I and S, form octagonal polygons and rectangular domains, respectively, while the majority P-blocks form domains with 8-coordination.

Increasing the C-volume fraction ($x \approx 1.45$) leads to a stable [8.6.4;8.6.6] pattern, while the morphologies of [8.8.4], [10.6.4;10.6.4;10.6.6], and [12.6.4] compete the stability with [8.6.4;8.6.6] in this region.

An interesting morphology, the [12.6.4] pattern, is observed in the region of $1.57 \leq x \leq 2.00$, whereas this morphology is a metastable phase for the star triblock

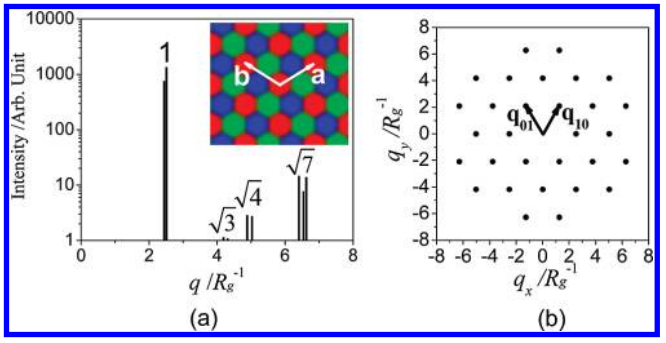

Figure 5. (a) Scattering intensity of pattern [6.6.6] plotted as a function of wavevectors q (in unit of R_g^{-1}). The inset is the corresponding schematic structure of [6.6.6] pattern. (b) 2-Dimensional scattering pattern of [6.6.6] tiling pattern.

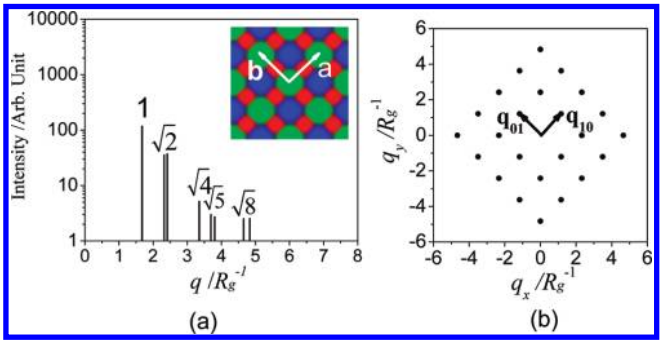

Figure 6. (a) Scattering profile of pattern [8.8.4]. The inset represents the corresponding schematic structure of [8.8.4] pattern. (b) Corresponding 2-dimensional scattering pattern.

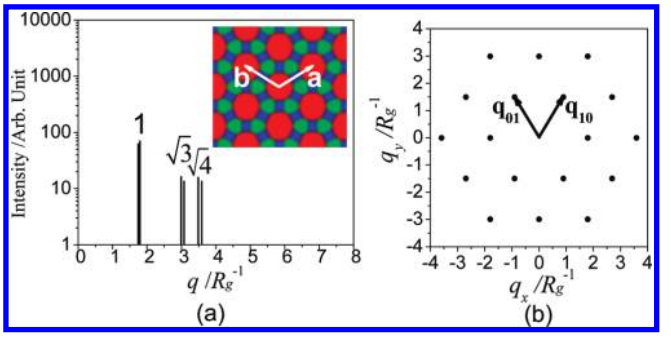

Figure 7. (a) Scattering profile of [12.6.4] pattern. The inset is the corresponding schematic structure of [12.6.4] pattern. (b) Corresponding 2-dimensional scattering pattern.

with symmetric interactions. In the experiments, the same structure was also observed in ISP star terpolymers with similar composition ratio of I:S:P = 1:1:1.9.[11,12] In this region, the SCFT calculations indicate that the patterns [10.6.4;10.6.4;10.6.6] and [8.6.4;8.6.6] are metastable phases.

(II). Scattering of Tiling Patterns. Identifying the symmetries of ordered phases obtained from theoretical calculations or simulations is a key step in the prediction of ordered structures self-assembled from block copolymers. In the real-space method of SCFT, density profiles of microphases are explicitly obtained. However it is still difficult to identify the symmetry group of the complex structures from these density profiles. This is especially true when the SCFT solutions correspond to defected structures typically obtained in large computational boxes. In the reciprocal-space method, the SCFT solutions are in the form of Fourier coefficients as a function of the wave vectors. For an ordered structure the wave vectors with nonzero coefficients correspond to the reciprocal lattice vectors of the structure. Therefore, it is straightforward to identify the symmetry of the ordered phase once the solutions of the SCFT equations are obtained in the reciprocal space. Detailed description of how to transform the wave vectors with nonzero coefficients into scattering patterns that can be compared with experiments is given previously in eq 32. In particular, Bragg diffraction occurs at the reciprocal lattice vectors, at which the scattering intensity exhibits scattering peaks.

As a simple example, the scattering intensity of a [6.6.6] tiling pattern is shown in Figure 5(a) as a function of the wavenumber q (in unit of R_g^{-1}). Bragg diffraction occurs at relative wave vectors

$$q/q^* = 1,\ \sqrt{3},\ \sqrt{4},\ \sqrt{7}$$

where q^* is the wave vector of the first-order peak. Note that each calculated scattering peak splits into several subpeaks, which is mainly due to the imperfect match between the computational lattice parameters and period of the ordered phases. For a typical [6.6.6] tiling pattern occurring at $D_x = 5.0R_g$, $D_y = 3.0R_g$, Figure 5b shows that the 2D pattern of the Bragg peaks, located at $(q_x = \pm k_x, q_y = \pm k_y)$, $(q_x = \pm 2k_x, q_y = 0)$, $(q_x = 0, q_y = \pm 2k_y)$, $(q_x = \pm 3k_x, q_y = \pm k_y)$, $(q_x = \pm k_x, q_y = \pm 3k_y)$, $(q_x = \pm 2k_x, q_y = \pm 2k_y)$, $(q_x = \pm 4k_x, q_y = 0)$, $(q_x = \pm 4k_x, q_y = \pm 2k_y)$, $(q_x = \pm 5k_x, q_y = \pm k_y)$, etc., where $k_x = 2\pi/D_x$, $k_y = 2\pi/D_y$. The magnitudes of the first scattering vectors, $|\mathbf{q}_{10}|$ and $|\mathbf{q}_{01}|$, are found to be $2.51R_g^{-1}$. The corresponding d-spacings, $d_{(10)}$ and $d_{(01)}$, can be calculated to be 2.50 R_g, using $d = 2\pi/|q|$. From these values, the real-space lattice vectors, $|\mathbf{a}|$ and $|\mathbf{b}|$, are found to be 2.89 R_g, and the angle between the two real lattice vectors is 120°. This calculated scattering pattern is in good agreement with the experimentally observed one.[12]

Figure 6a shows the scattering profile of the [8.8.4] tiling pattern. The scattering peaks are located at

$$q/q^* = 1,\ \sqrt{2},\ \sqrt{4},\ \sqrt{5},\ \sqrt{8}$$

where $q^*$is the peak position of the first-order scattering. This scattering intensity profile exhibits a 4-fold symmetry, consistent with the [8.8.4] structure. From the SCFT results, it is found that this pattern occurs at $D_x = 5.40R_g$ and $D_y = 5.20R_g$, resulting in $|\mathbf{q}_{01}| = |\mathbf{q}_{10}| = 1.68R_g^{-1}$, $|\mathbf{a}| = |\mathbf{b}| = 3.75R_g$, and the angle between two real lattice vectors is 90°. Figure 6b illustrates the 2D scattering pattern of such [8.8.4] tiling pattern, in which the 01, 02, 11, 12, and 22 reflections are clearly observed. This characteristic of the [8.8.4] pattern is consistent with the experimental results.[12]

Finally the scattering profile of the [12.6.4] tiling pattern is shown in Figure 7(a). The scattering profile has peaks at

$$q/q^* = 1,\ \sqrt{3},\ \sqrt{4}$$

These ratios indicate a structure of 6-fold symmetry. For a typical [12.6.4] structure occurring at $D_x = 7.00R_g$, $D_y = 4.20R_g$, Figure 7(b) shows the 2D scattering pattern, where the Bragg peaks appear at $(q_x = \pm k_x, q_y = \pm k_y)$, $(q_x = \pm 2k_x, q_y = 0)$, $(q_x = 0, q_y = \pm 2k_y)$, $(q_x = \pm 3k_x, q_y = \pm k_y)$, $(q_x = \pm 4k_x, q_y = 0)$ and $(q_x = \pm 2k_x, q_y = \pm 2k_y)$, etc., where $k_x = 2\pi/D_x$, $k_y = 2\pi/D_y$. The amplitudes of the scattering vectors, $|\mathbf{q}_{10}|$ and $|\mathbf{q}_{01}|$, are 1.80 R_g^{-1} and 1.74 R_g^{-1}, respectively. Consequently, the angle between the two scattering vectors is 59°, indicating an angle of 121° between the two real lattice vectors. The amplitudes of the two real lattice vectors, $|\mathbf{a}|$ and

$|\mathbf{b}|$, are found to be 4.08 R_g and 5.60 R_g, while the d-spacings, $d_{(01)}$ and $d_{(10)}$, are $3.60R_g^{-1}$ and $3.50R_g^{-1}$, respectively.

IV. Conclusions

The phase behavior of ABC star-shaped terpolymers has been investigated by self-consistent field theory (SCFT) in reciprocal-space. Motivated by previous experimental and simulation studies, attention has been focused on the ordering of 2D phases or tiling patterns self-assembled from ABC star terpolymers. The SCFT calculations predict that a variety of tiling morphologies, including the [8.8.4], [6.6.6], [8.6.4;8.6.6], [10.6.4;10.6.4;10.6.6], [12.6.4], and [8.6.4;8.8.4;12.6.4;12.8.4] tiling patterns, can occur in ABC star terpolymers. Except for the [8.6.4;8.8.4;12.6.4;12.8.4] tiling pattern, these ordered phases have been observed in previous experiments and simulations.

Two typical ABC star terpolymers with symmetric and asymmetric interaction parameters are investigated. For the terpolymers with symmetric interactions, a triangle phase diagram is constructed and the phase behavior of the $A_{1.0}B_{1.0}C_x$ star terpolymers is presented in detail. The phase transition is predicted to occur in a sequence of [8.8.4], [6.6.6], [8.6.4;8.6.6], [10.6.4;10.6.4;10.6.6] with increasing volume fraction f_C from 0.21 to 0.50 ($0.53 \leq x \leq 2.02$).

For the star terpolymers with asymmetric interactions appropriate to ISP star polymer, a series of star terpolymers with composition $A_{1.0}B_{1.0}C_x$ has been examined in detail. Significant changes in the phase behavior have been observed. As the volume fraction of the C-block is increased, the equilibrium ordered phases are predicted to occur in the order of: $[8.8.4]^1$, $[8.8.4]^2$, [8.6.4;8.6.6], and [12.6.4].

Furthermore, the scattering intensity profiles of three ordered phases, the [6.6.6], [8.8.4], and [12.6.4] tiling patterns, are calculated from our mean-field solutions. Good agreement between the calculated scattering patterns with those observed in experiments has been reached.

To simplify the calculation and focusing on the tiling patterns, the SCFT calculation in this paper was carried out only in 2D space; however, extension to 3D space is straightforward and without any limitation. In fact, various interesting 3D ordered morphologies of ABC star terpolymers have been collected, using the present Fourier-space method. The ordering of ABC star terpolymers in 3D space will be the main topic of our next publication.

Acknowledgment. We express thanks for the financial support from the National Basic Research Program of China (Grant No. 2005CB623800) and National Natural Science Foundation of China (Grants No. 20625413, No. 20874021, and No. 20990231). A.-C.S. acknowledges support from the Natural Science and Engineering Research Council (NSERC) of Canada.

References and Notes

(1) Hamley, I. W. *The Physics of Block Copolymers*; Oxford University Press: Oxford, U.K., 1998.
(2) Parka, C.; Yoon, J.; Thomas, E. L. *Polymer* **2003**, *44*, 6725.
(3) Hamley, I. W., Ed. *Developments in Block Copolymer Science and Technology*; Wiley: New York, 2004.
(4) Abetz, V.; Simon, P. F. W. *Adv. Polym. Sci.* **2005**, *189*, 125.
(5) Tyler, C. A.; Morse, D. C. *Phys. Rev. Lett.* **2005**, *94*, 208302.
(6) Takenaka, M.; Wakada, T.; Akasaka, S.; Nishitsuji, S.; Saijo, K.; Shimizu, H.; Kim, M. I.; Hasegawa, H. *Macromolecules* **2007**, *40*, 4399.
(7) (a) Auschra, C.; Stadler, R. *Macromolecules* **1993**, *26*, 2171. (b) Stadler, R.; Auschra, C.; Beckmann, J.; Krappe, U.; Voigt-Martin, I.; Leibler, L. *Macromolecules* **1995**, *28*, 3080. (c) Krappe, U.; Stadler, R.; Voigt-Martin, I. *Macromolecules* **1995**, *28*, 4558. (d) Stocker, W.; Beckmann, J.; Stadler, R.; Rabe, J. *Macromolecules* **1996**, *29*, 7502. (e) Breiner, U.; Krappe, U.; Abetz, V.; Stadler, R. *Macromol. Chem. Phys.* **1997**, *198*, 1051. (f) Breiner, U.; Krappe, U.; Thomas, E. L.; Stabler, R. *Macromolecules* **1998**, *31*, 135.
(8) (a) Shefelbine, T.; Vigild, M.; Matsen, M.; Hajduk, D.; Hillmyer, M.; Cussler, E.; Bates, F. *J. Am. Chem. Soc.* **1999**, *121*, 8457. (b) Bailey, T. S.; Hardy, C. M.; Epps, T. H.III; Bates, F. S. *Macromolecules* **2002**, *35*, 7007. (c) Epps, T. H.; Bailey, T. S.; Waletzko, R. S.; Bates, F. S. *Macromolecules* **2003**, *36*, 2873. (d) Epps, T. H.; Cochran, E. W.; Hardy, C. M.; Bailey, T. S.; Waletzko, R. S.; Bates, F. S. *Macromolecules* **2004**, *37*, 7085. (e) Epps, T. H.; Cochran, E. W.; Bailey, T. S.; Waletzko, R. S.; Hardy, C. M.; Bates, F. S. *Macromolecules* **2004**, *37*, 8325. (f) Bates, F. S. *MRS Bull.* **2005**, *30*, 525. (g) Epps, T. H.III; Bates, F. S. *Macromolecules* **2006**, *39*, 2676. (h) Chatterjee, J.; Jain, S.; Bates, F. S. *Macromolecules* **2007**, *40*, 2882. (i) Tyler, C. A.; Qin, J.; Bates, F. S.; Morse, D. C. *Macromolecules* **2007**, *40*, 4654.
(9) (a) Matsushita, Y.; Tamura, M.; Noda, I. *Macromolecules* **1992**, *27*, 3680. (b) Mogi, Y.; Kotsuji, H.; Kaneko, Y.; Mori, K.; Matsushita, Y.; Noda, I. *Macromolecules* **1992**, *25*, 5408. (c) Mogi, Y.; Mori, K.; Matsushita, Y.; Noda, I. *Macromolecules* **1992**, *25*, 5412. (d) Mogi, Y.; Mori, K.; Kotsuji, H.; Matsushita, Y.; Noda, I.; Han, C. C. *Macromolecules* **1993**, *26*, 5169. (e) Mogi, Y.; Nomura, M.; Kotsuji, H.; Ohnishi, K.; Matsushita, Y.; Noda, I. *Macromolecules* **1994**, *27*, 6755.
(10) Grunbaum, B.; Shephard, G. C. *Tilings and Patterns*; Freeman: New York, 1986.
(11) Takano, A.; Wada, S.; Sato, S.; Araki, T.; Hirahara, K.; Kazama, T.; Kawahara, S.; Isono, Y.; Ohno, A.; Tanaka, N.; Matsushita, Y. *Macromolecules* **2004**, *37*, 9941.
(12) Hayashida, K.; Kawashima, W.; Takano, A.; Shinohara, Y.; Amemiya, Y.; Nozue, Y.; Matsushita, Y. *Macromolecules* **2006**, *39*, 4869.
(13) Takano, A.; Kawashima, W.; Noro, A.; Isono, Y.; Tanaka, N.; Dotera, T.; Matsushita, Y. *J. Polym. Sci., Part B: Polym. Phys.* **2005**, *43*, 2427.
(14) Hayashida, K.; Takano, A.; Arai, S.; Shinohara, Y.; Amemiya, Y.; Matsushita, Y. *Macromolecules* **2006**, *39*, 9402.
(15) Huckstadt, H.; Gopfert, A.; Abetz, V. *Macromol. Chem. Phys.* **2000**, *201*, 296.
(16) Gemma, T.; Hatano, A.; Dotera, T. *Macromolecules* **2002**, *35*, 3225.
(17) Huang, C.-I.; Fang, H.-K.; Lin, C.-H. *Phys. Rev. E* **2008**, *77*, 031804.
(18) Fredrickson, G. H. *The Equilibrium Theory of Inhomogeneous Polymers*; Oxford University Press: Oxford, U.K., 2006.
(19) Shi, A.-C. In *Development in Block Copolymer Science and Technology*; Hamley, I. W., Ed.; Wiley: New York, 2004.
(20) Edwards, S. F. *Proc. Phys. Soc.* **1965**, *85*, 613.
(21) (a) Helfand, E. *J. Chem. Phys.* **1975**, *62*, 999–1005. (b) Helfand, E. *J. Macromolecules* **1975**, *8*, 552.
(22) Hong, K. M.; Noolandi, J. *Macromolecules* **1981**, *14*, 727.
(23) Matsen, M. W.; Schick, M. *Phys. Rev. Lett.* **1994**, *72*, 2660.
(24) Drolet, F.; Fredrickson, G. H. *Phys. Rev. Lett.* **1999**, *83*, 4317.
(25) Tzeremes, G.; Rasmussen, K. Ø.; Lookman, T.; Saxena, A. *Phys. Rev. E* **2002**, *65*, 041806.
(26) Tyler, C. A.; Qin, J.; Bates, F. S.; Morse, D. C. *Macromolecules* **2007**, *40*, 4654.
(27) Guo, Z. J.; Zhang, G. J.; Qiu, F.; Zhang, H. D.; Yang, Y. L.; Shi, A.-C. *Phys. Rev. Lett.* **2008**, *101*, 028301.
(28) The validity of rectangular unit cell is based on the observation that till now the unit cells of all ordered phases of block copolymers found in experiments are orthogonal. However, it is still possible to find nonrectangular phases in block copolymers later. It is our next endeavor to develop corresponding numerical method for cases with more generic unit cell, which will be proven more powerful for prediction of phases in block copolymers.
(29) Chaikin, P. M.; Lubensky, T. C. *Principles of Condensed Matter Physics*; Cambridge University Press: Cambridge, U.K., 1995.
(30) The relaxation method is an iteration method used to find solutions of the SCFT equations. A detailed description of such iteration method can be found in, for example: Laradji, M.; Shi, A. C.; Noolandi, J.; Desai, R. C. *Macromolecules* **1997**, *30*, 3242.